ORIGINAL ARTICLE

Wen-Shao Chang · Min-Fu Hsu

Rotational performance of traditional Nuki joints with gap II: the behavior of butted Nuki joint and its comparison with continuous Nuki joint

Abstract Nuki joints are often used in oriental carpentry. Various types of Nuki joints have different structural characteristics, which needs further investigation. This article proposes a theoretical model for butted Nuki joints and reports verification of the model by 21 full-scale tests. We then compare the mechanical behaviors of butted Nuki joints with continuous Nuki joints by using the theoretical models proposed in this article and in a previous report. The results show that the initial stiffness and moment resistance of butted Nuki joints are much lower than continuous joints, and the butted Nuki joints have larger initial rotation without any moment resistance. The results of this study help us understand the structural behavior, and to estimate the structural characteristics of butted Nuki joints when carrying out the structural analyses.

Key words Nuki joints · Semirigid connections · Traditional timber structures

Introduction

Timber connections play a crucial role on the structural behavior of timber constructions, as they usually affect the internal force distribution in the whole structure. The Nuki joint is one of the simplest methods of connecting the structural components to create a shelter and involves penetrating one element through another. However, the simplicity is not the only advantage of Nuki joints; they have good ductility because they use both embedment and friction to resist the moment force. Hence, the Oriental carpentries, such as those in Taiwan, Japan, and China, often use Nuki joints to connect the posts and beams in timber structures. The Japanese Nuki joints are usually wedged to prevent initial rotation, while a gap is usually acceptable in Taiwan-

ese carpentry. This wedge stabilization results in different structural behaviors of Nuki joints in Japan and Taiwan.

Recent years have seen increased attention being given to the structural behavior of Japanese Nuki joints.[1–4] On the contrary, little has been published on the behavior of Taiwanese Nuki joints. The results of a field survey show that Nuki joints in Taiwan comprise three various types, which are the continuous, butted, and dovetail types, as shown in Fig. 1. These Nuki joints have different mechanisms in connecting the beams inside the columns, but the appearances are identical. One of the primary research questions to be addressed is the difference of these Nuki joints in mechanical performance.

Our previous study[5] investigated the rotational behavior of continuous-type Nuki joints subjected to moment action. However, the mechanical behavior of butted and dovetail Nuki joints are still in question. The present study explored the rotational performance of butted Nuki joints by comparing the theoretical model established in this study with the experimental results. The differences in behavior of these two types of Taiwanese Nuki joints, when subjected to moment action, are discussed.

Rotational behavior

A previous study[6] showed that the beams of butted Nuki joints do not rotate synchronically, that is, the separate beams do not affect each other. Thus, in this study, we only employ a beam on one side of the joint to demonstrate the rotational behavior of butted Nuki joints.

Figure 2 illustrates the behaviors of a butted Nuki joint subjected to moment action. Due to the craftsmanship error and constructional practice, the carpenters usually leave a gap between the beam and the slot in the column as shown in Fig. 2a. The gap leads to an initial rotation, θ_0, without any moment resistance. Not until the stage of Fig. 2b, does the beam act as rigid-body rotation and behave as a hinge. The moment resistance starts to show up during the stage of Fig. 2b and increases afterward. As the rotation increases

W.-S. Chang (✉) · M.-F. Hsu
Department of Architecture, National Cheng Kung University,
No. 1, University Road, Tainan City 701, Taiwan
Tel. +886-6-275-7575; Fax +886-6-237-4680
e-mail: wen_shao_chang@yahoo.com.tw

Fig. 1a–c. Various types of Taiwanese Nuki joints. **a** Continuous type, **b** dovetail type, and **c** butted type
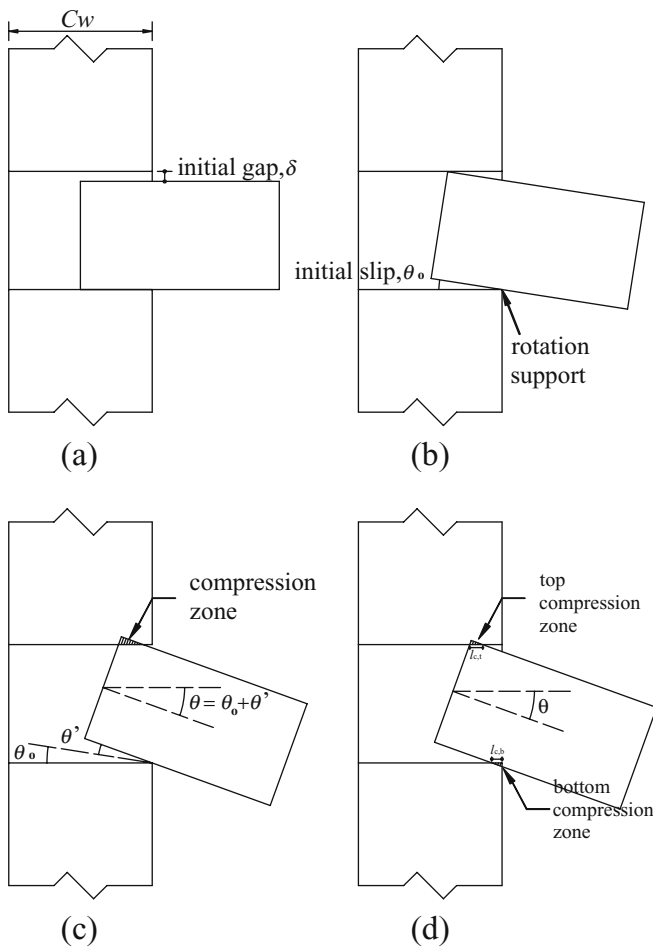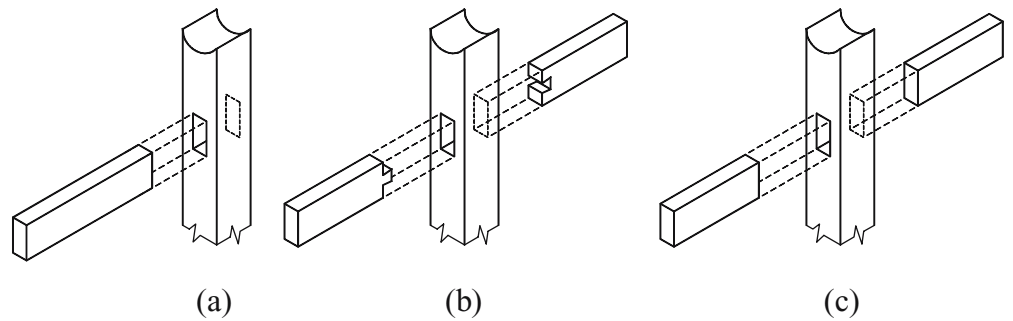

Fig. 2a–d. Rotational progress of butted Nuki joints. **a** Initial situation, without rotation, **b** rotation without resistance, **c** increasing the rotation leads to embedment at the top, **d** the beam sinks so that the resultant force at the top and bottom will be equivalent

to θ', the compressive zone increases as illustrated in Fig. 2c. In this stage, the beam sinks downward after which the compressive zone in the bottom takes place as shown in Fig. 2d. In the stage of Fig. 2d, the resultant force due to embedment at the top of the beam will be equivalent to that at the bottom, and friction resistances occur at both the top and bottom part of the embedment. In this report, $l_{c,t}$ and $l_{c,b}$ are used to describe the compressive lengths at the top and bottom parts, respectively, as shown in Fig. 2d. From the previous discussion we see that the rotation center of

abutted Nuki joint varies with rotation of the beam after the stage of Fig. 2b, which is significantly different from the case of a continuous Nuki joint.

Theory

To develop the theoretical model to investigate the moment–rotation behavior of butted Nuki joints, five assumptions were made in this study:

1. Hooke's law is applicable in the development of theory in this study.
2. The material properties can be described by a bilinear model.
3. The modulus of elasticity (MOE) of wood parallel to the grain is 20 times the MOE perpendicular to the grain. This is suitable for softwood.
4. The rotation θ can be divided into two parts, including the gap-induced initial rotation θ_0, which occurs first, and rotation θ' that occurs after this stage. $\theta = \theta_0 + \theta'$, as shown in Fig. 2.
5. Although the friction coefficient is usually affected by many factors, such as species, fiber orientation, moisture content, roughness of contact surface, and relative velocity of friction, the friction coefficient is assumed to be constant in this study to simplify the calculation.

Assuming that the moment resistance of the butted Nuki joint is provided by the embedment and friction between beam and column, the following relationship can be expressed

$$M_{\text{total}} = M_{\text{em}} + M_{\text{fric}} \tag{1}$$

in which the M_{em} and M_{fric} represent the moment resistance provided by embedment and friction, respectively.

The geometry of half butted Nuki joint with a rotation θ is demonstrated in Fig. 3. To simplify the calculation concerning the geometries, we let

$$\theta = \theta_o + \theta', \quad L = \sqrt{Bd^2 + \left(\frac{1}{2}Cw\right)^2}, \text{ and } \phi = \tan^{-1}\frac{Bd}{\frac{1}{2}Cw} \tag{2}$$

where Bd represents the beam depth and Cw is the column width.

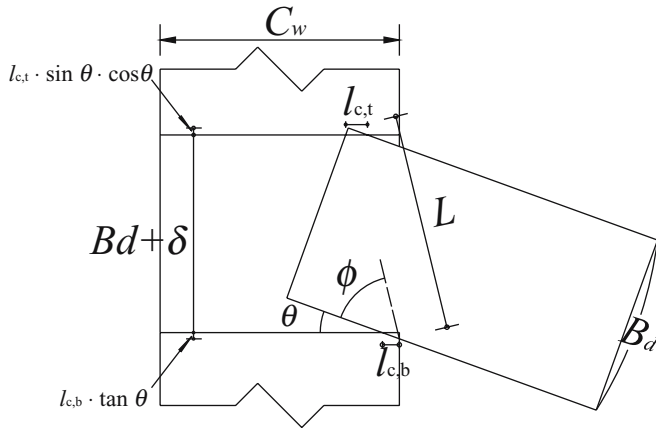For a beam with rotation θ, the maximum strains at the top and bottom compression zones can be expressed as:

Fig. 3. Geometry of beam under rotation θ

(a)

(b)

Fig. 4a, b. Free body diagram of joint subjected to moment M with rotation θ. **a** Entire joint, **b** free body diagram

$$\begin{cases} \varepsilon_{\max,t} = \dfrac{l_{c,t}}{Bd} \cdot \sin\theta \cdot \cos^2\theta \\[2mm] \varepsilon_{\max,b} = \dfrac{l_{c,b}}{Bd} \cdot \sin\theta \end{cases} \tag{3}$$

According to Hooke's law, the maximum stress in linear stage for the top and bottom compression zones will be:

$$\begin{cases} \sigma_{\max,t} = \varepsilon_{\max,t} \cdot E_\perp \cdot \beta(\theta) \\ \sigma_{\max,b} = \varepsilon_{\max,b} \cdot E_\perp \cdot \beta(\theta) \end{cases} \tag{4}$$

where $E_\perp$ represents the MOE of the beam perpendicular to the grain. By setting the coefficient $n = 3.1$, which is suitable for Chinese cedar[7] (*Cunninghamia lanceolata*), the Hankinson's formula, $\beta(\theta)$, can be expressed in the form of:

$$\beta(\theta) = \frac{20}{20 \cdot \cos^{3.1}\theta + \sin^{3.1}\theta} \tag{5}$$

The resultant force induced by compression at the top and bottom compressive zones in the linear stage can be respectively written as:

$$\begin{aligned} f_{res,t}(\theta) &= \frac{1}{2} \cdot l_{c,t} \cdot Bw \cdot \varepsilon_{\max,t} \cdot E_\perp \cdot \beta(\theta) \\ &= \frac{1}{2} \cdot l_{c,t}{}^2 \cdot \frac{Bw \cdot E_\perp}{Bd} \cdot \beta(\theta) \cdot \sin\theta \cdot \cos^2\theta \end{aligned} \tag{6}$$
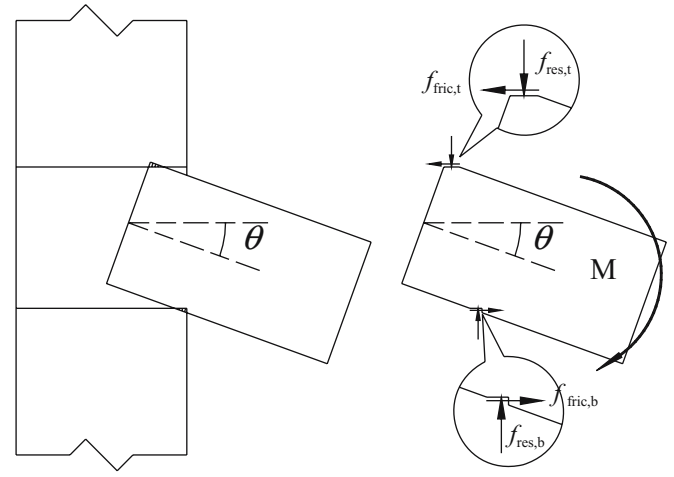
$$\begin{aligned} f_{res,b}(\sigma) &= \frac{1}{2} \cdot l_{c,b} \cdot Bw \cdot \varepsilon_{\max,b} \cdot E_\perp \cdot \beta(\theta) \\ &= \frac{1}{2} \cdot l_{c,b}{}^2 \cdot \frac{Bw \cdot E_\perp}{Bd} \cdot \beta(\theta) \cdot \sin\theta \end{aligned} \tag{7}$$

where Bw represents the beam width.

Note that in the free body diagram in Fig. 4b, the resultant force at the top compression zone should be equivalent to that at the bottom compression zone. Thus, we can obtain:

$$f_{res,t} = f_{res,b} \tag{8}$$

In such a case, the relationship between the compression lengths at the top and bottom zones can be obtained:

$$l_{c,b} = l_{c,t} \cdot \cos\theta \tag{9}$$

As shown in Fig. 3, to obtain the compression lengths at the top and bottom compression zones, the following geometric condition can be used:

$$Bd + \delta + l_{c,b} \cdot \tan\theta + l_{c,t} \cdot \sin\theta \cdot \cos\theta = L \cdot \sin(\theta + \phi) \tag{10}$$

According to Eq. 10, the compression length can be yielded as:

$$l_{c,t} = \frac{L \cdot \sin(\theta + \phi) - Bd - \delta}{\sin\theta \cdot (1 + \cos\theta)} \tag{11}$$

The lever arm of the embedment portion, L_{em}, can be written in the form of:

$$\begin{aligned} L_{em}(\theta) &= L \cdot \cos(\theta + \phi) - l_{c,t} \cdot \left(\frac{2}{3} \cdot \cos^2\theta - \frac{1}{3}\right) - \frac{1}{3} \cdot l_{c,b} \\ &= L \cdot \cos(\theta + \phi) - \frac{1}{3} \cdot l_{c,t} \cdot [2 \cdot \cos^2\theta + \cos\theta - 1] \end{aligned} \tag{12}$$

The moment resistance provided by embedment on the beam is a function of beam rotation and can be expressed by:

$$M_{em}(\theta) = L_{em}(\theta) \cdot f_{res,t}(\theta) \tag{13}$$

The resultant forces induced by friction can be expressed as:

$$\begin{cases} f_{fric,t}(\theta) = \mu \cdot f_{res,t} \\ f_{fric,b}(\theta) = \mu \cdot f_{res,b} \end{cases} \tag{14}$$

where μ is the friction coefficient for wood–wood surfaces.

Only limited reports of the value of friction coefficient on wood–wood surface are given in the literature. McKenzie and Karpovic[8] pointed out that the sliding friction coefficient for wood–wood surfaces ranges from 0.1 to 0.65. Murase[9] indicated the value of 0.58 for species of western

hemlock (*Tsuga heterophylla*). The value of 0.6 was used in this study because it is reasonable and corresponds to the experimental results.

The lever arm for friction effect, L_{fric}, is equivalent to the overall height of the slot:

$$L_{fric} = Bd + \delta \tag{15}$$

where δ represents the gap between the beam and the slot in the column. The moment resistance provided by the friction effect can be obtained by:

$$M_{fric}(\theta) = L_{fric} \cdot f_{fric}(\theta) \tag{16}$$

The moment resistance of butted Nuki joints can be obtained by substituting Eqs. 13 and 16 into Eq. 1.

Materials and methods

To clarify the theoretical model proposed in the previous section, a total of 21 full-scale butted Nuki joints were tested. Our previous report[5] showed that the factors that affect the mechanical performance of Nuki joints are beam depth (*Bd*), beam width (*Bw*), column width (*Cw*), and MOE of beam perpendicular to the grain. Thus, the geometries and material properties of the specimens tested are listed in Table 1. The experimental setup is illustrated in Fig. 5. The material used for the specimens was Chinese Fir. The moisture content of the wood specimens was controlled to below 19%, and specimens were stored in the laboratory with good natural ventilation prior to experiments. Compressive tests were conducted on the beam of each specimen to obtain the MOE perpendicular to the grain before the experiments. Monotonic loads were applied by displacement control at a speed of 0.5 mm/min at the loading point,

which is equal to 0.0125 rad/min for rotation. The experiments were terminated when the maximum stroke of hydraulic jack or maximum rotation of 0.16 rad was reached.

Results and discussion

Failure mode

Similar failure modes occurred in the 21 specimens, including slight friction and embedment failures on the beam. No mechanical failure was observed on the column. As shown in Fig. 6, the end of the beam positioned inside the column was polished due to the friction. This might result in changing of the friction coefficient at the contact surfaces. In the other words, the friction coefficient might change with rotation. Tiny compression failure took place on beam element at the location where the beam contacts the edge of the slot in the column, as shown in Fig. 7. Comparing the observed failures with those found in continuous Nuki joints, the damage of butted joints is much less and no shear failure perpendicular to the grain occurs.

Table 1. Experimental design table

Experiment	Cw (mm)	Bd (mm)	Bw (mm)	$E_\perp$ (Gpa)		Replicas
				Mean	SD	
BN-A	120	120	60	0.372	0.039	3
BN-B	120	120	90	0.369	0.040	3
BN-C	180	180	60	0.394	0.056	3
BN-D	120	180	90	0.368	0.060	3
BN-E	180	120	60	0.367	0.037	3
BN-F	150	120	90	0.315	0.072	3
BN-G	180	180	90	0.393	0.060	3

Cw, Column width; *Bd*, beam depth; *Bw*, beam width; $E_\perp$ modulus of elasticity perpendicular to the grain
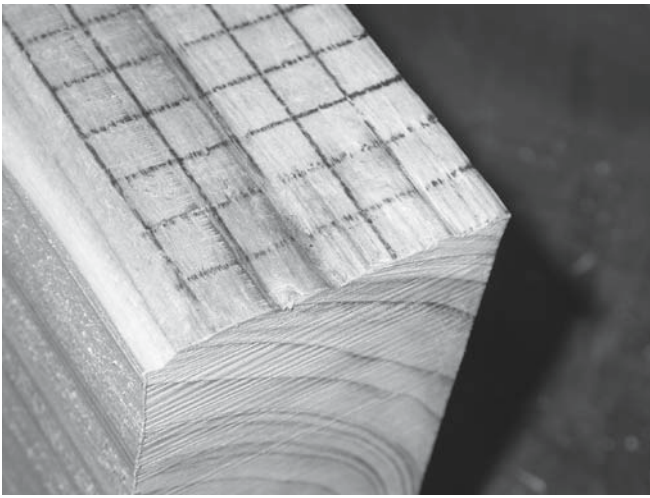
Fig. 5. Experimental setup
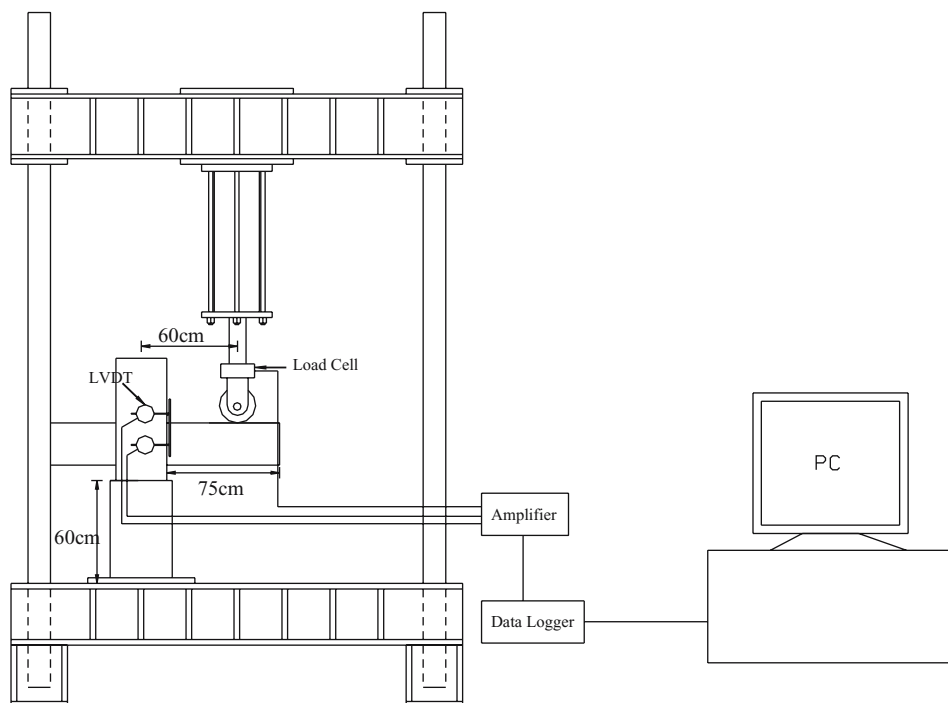
Fig. 6. The end of the beam was polished due to friction between beam and column
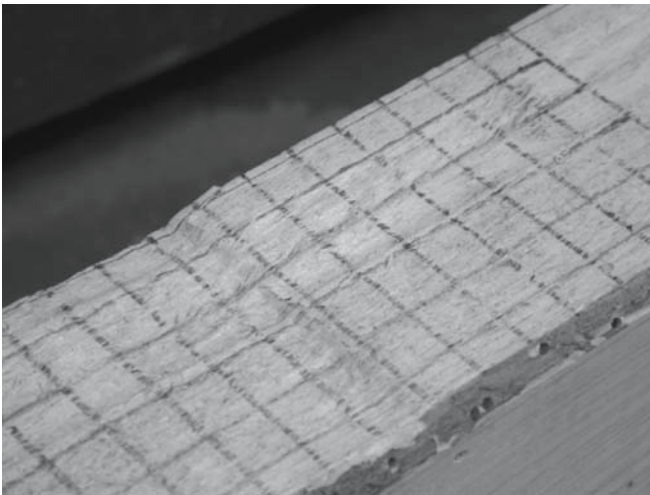

Fig. 7. Embedded failure at beam following contact with column

Verification

Figure 8 compares the $M - \theta$ relationships obtained from experimental results with those from theoretical models proposed in this study. It should be noted that the model considers the gap, and so the initial slip of the joint can be observed not only in experimental data but also in the theoretical model. Satisfactory agreement was found between the analytical and experimental results, especially in the elastic stage. The error at larger rotation may have been caused by the assumption that the friction coefficient is constant becoming unrealistic; the friction coefficient may well have been affected by the inclined contact surfaces as pointed out in the literature[8] and polishing of contact surfaces on the beam may have occurred. For more accurate prediction, especially in the inelastic stage, further consideration needs to be given to possible changes in the friction coefficient for wood–wood surfaces with inclined contact.
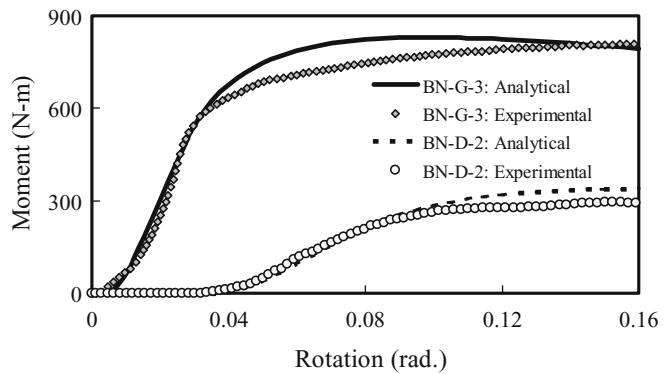

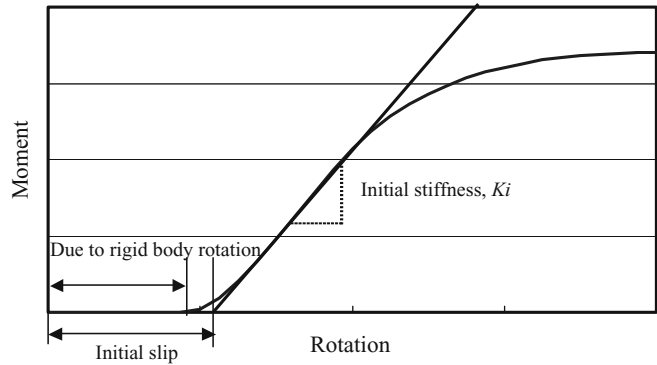**Fig. 8.** Comparisons of analytical and experimental results

Fig. 9. Typical $M - \theta$ curve of timber joints
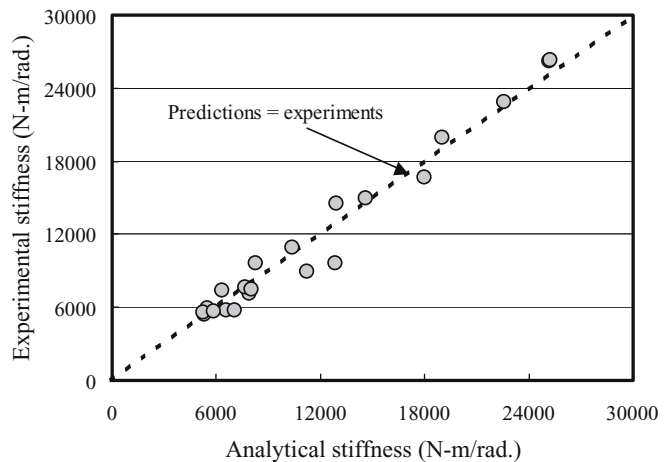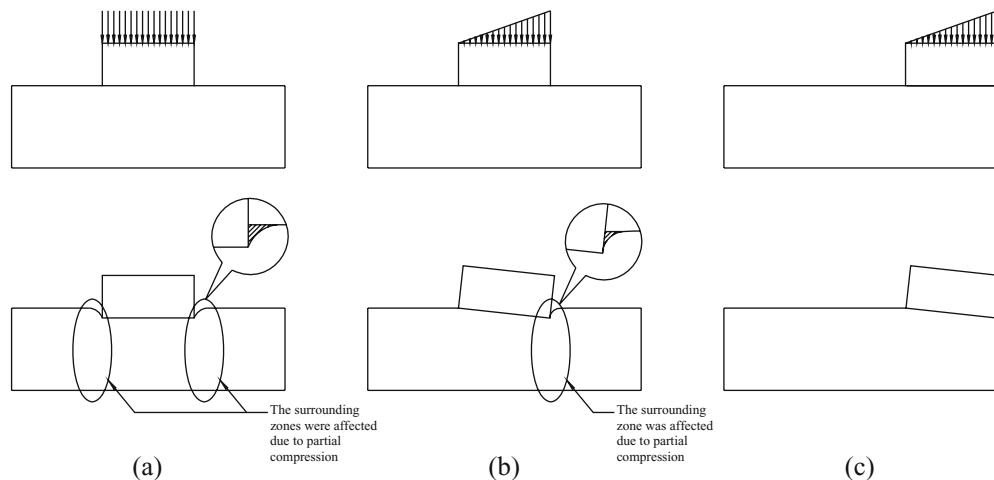

Fig. 10. Comparison of initial stiffness obtained from analytical and experimental results

The initial stiffness, K_i, of the Nuki joint is defined in Fig. 9 as the slope of the $M - \theta$ curve after the initial slip stage. Figure 10 demonstrates the comparison of initial stiffness obtained from experiments and analytical models. Good agreement can be found, with an average error of 2.36%. The comparison can manifest the assumptions made previously in the elastic stage.

Fig. 11a–c. Various situations of partial compression. **a** Partial compression with solid block compressed vertically, **b** partial compression with solid block compressed on one side, **c** partial compression with solid block compressed at the edge of the base material

The surrounding zones were affected due to partial compression

The surrounding zone was affected due to partial compression

(a)   (b)   (c)

Feasibility of Hooke's law

From Fig. 4 it is apparent that partial compression occurs at the area where the beam contacts the column, which might lead to significant error if this effect is ignored. Previous sections showed acceptable agreement between results obtained from theoretical calculations and experiments, which in some way shows the feasibility of Hooke's law and its application.

There are several different situations (Fig. 11), for which we should consider partial compression. In cases (a) and (b), the error will be induced once partial compressions are not considered. In case (c), the error will not be significant even if partial compression is not taken into account. The hatched areas of situations (a) and (b) in Fig. 11 represent the error of the situation. It is obvious that situation (b) has less error than case (a) in using Hooke's law in the theory, which might be the reason that acceptable agreement was found in the previous section.

Comparison with continuous Nuki joints

The theoretical models proposed in this study and our previous report[5] have showed the validity of the assumptions and the models. Hence, this article compares the mechanical behavior of butted and continuous Nuki joints by using the models we developed. We first assumed that the butted and continuous Nuki joints have identical geometries and material properties, where the beam section was 180×60 mm, the column section was 180×180 mm, and the gap was 2 mm wide. The MOE of the beam perpendicular to the grain was assumed to be 0.4 Gpa. Figure 12 compares the $M - \theta$ relationships of continuous and butted Nuki joints calculated from the theoretical models, and shows significant difference between the two joints in mechanical performance. The initial stiffness and moment resistance decrease dramatically once the beam becomes discontinuous and just butted together. In the example taken in this study, the initial stiffness of Nuki joints drop to 21.3% of the origin once the carpenters adopted the butted Nuki joints rather than using the continuos Nuki joints. This is not desirable.
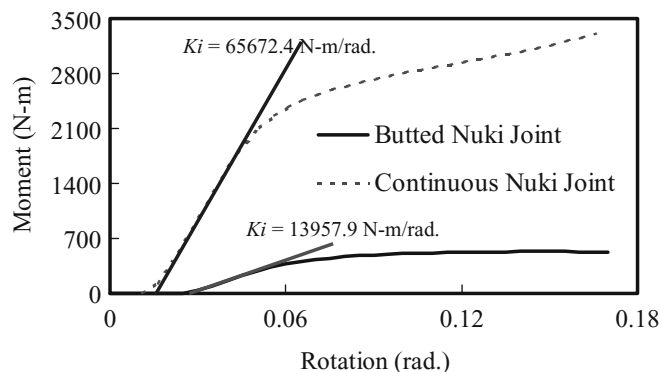

$Ki = 65672.4$ N-m/rad.

Butted Nuki Joint

Continuous Nuki Joint

$Ki = 13957.9$ N-m/rad.

Fig. 12. Comparison of moment–rotation curves for butted and continuous Nuki connections

Another noteworthy phenomenon is that the moment resistance of butted Nuki connections starts to show up at a rotation that is approximately double that in the continuous case. The gap between the beam and the slot in the column will result in rigid body rotation, θ_0, of beam, as shown in Figs. 2 and 9. The initial rotations of butted and continuous Nuki joints can be respectively represented by:

$$\theta_{0,\text{butted}} = \tan^{-1} \frac{2 \cdot \delta}{Cw} \tag{17}$$

$$\theta_{0,\text{continuous}} = \tan^{-1} \frac{\delta}{Cw} \tag{18}$$

Thus, it is reasonable for butted Nuki joints to have larger rotation without any moment resistance, and these connections are more sensitive to the gaps between beams and the slots in columns.

Conclusions

This study proposed a theoretical model to explore the mechanical behavior of butted Nuki joints; this was verified by a total of 21 full-scale tests. The experiments showed that the butted Nuki joints were subjected to only slight damage

compared with that observed in the continuous Nuki connections. The butted Nuki connections showed considerably lower initial stiffness and moment resistance than the continuous Nuki joints. We also found that the butted Nuki connections were more sensitive to the gaps, which mean large initial rotation. This study not only appears to support the superiority of the mechanical performance of continuous Nuki joints, but also reveals the necessity of research effort to be devoted to the reinforcement of butted Nuki joints in the future.

References

1. Kitamori A, Kato Y, Kataoka Y, Komatsu K (2003) Proposal of a mechanical model of beam–column "Nuki" joints in traditional timber structures (in Japanese). Mokuzai Gakkaishi 49:179–186

2. Kato Y, Komatsu K, Kitamori A (2003) Role of wedges on the stiffness and strength of column–"Nuki" (narrow beam) joints in traditional timber frame structures (in Japanese). Mokuzai Gakkaishi 49:84–91

3. Kitamori A, Komatsu K, Kato Y, Kataoka Y (2002) Effect of the degree of wedge fixation on the rotational behaviour of beam–column "Nuki" joint. Proceedings of 7th World Conference on Timber Engineering, Shah Alam, Malaysia, pp173–182

4. Inayama M (1995) Design of compressive strain-resistant connections (Nuki) (in Japanese). Kenchiku-Gijutu 547:106–111

5. Chang WS, Hsu MF, Komatsu K (2006) Rotational performance of traditional Nuki joints with gap I: theory and verification. J Wood Sci 52:58–62

6. Chang WS (2005) On rotational performance of traditional Chuan-Dou timber joints in Taiwan. Ph.D. dissertation, National Cheng Kung University, Tainan, Taiwan

7. Wang SY (1993) Wood physics (in Chinese). National Institute of Compilation and Translation, Taipei, pp 524–525

8. McKenzie WM, Karpovic H (1968) Frictional behaviour of wood. Wood Sci Technol 2:138–152

9. Murase Y (1984) Friction of wood sliding on various materials. J Fac Agric Kyushu Univ 28:147–160